THE JOURNAL OF PHYSICAL CHEMISTRY C
A JOURNAL OF THE AMERICAN CHEMICAL SOCIETY

pubs.acs.org/JPCC
Article

Electrochemical Oxidative Desorption of Adsorbed Sulfur Species on (111) Surfaces of Single Crystals of Pure Pt and Pt-Based Bimetallic Alloys

Makoto Aoki, Tamao Shishido, Tetsuro Morooka, Takuya Nakanishi, and Takuya Masuda*

Cite This: J. Phys. Chem. C 2025, 129, 2122−2131
Read Online

ABSTRACT: The adsorption/desorption behavior of sulfur species at the (111) surfaces of pure Pt and various Pt-based bimetallic alloys, denoted as Pt_3M (M = Co, Cu, Fe, Pd), was investigated by electrochemical measurements and X-ray photoelectron spectroscopy (XPS). After the adsorption of elemental sulfur, the current responses characteristic of the adsorption/desorption of hydrogen and hydroxyl species at the sulfur-free bare (111) surfaces completely disappeared, and a doublet peak corresponding to the elemental sulfur appeared in the S 2p region of XPS spectra. The characteristic current responses gradually recovered, simultaneously with the decrease of the S 2p peak, by repeating the potential cycling between −0.2 and 0.8 V vs Ag/AgCl, indicating the oxidative desorption of S species. Except for the $Pt_3Pd(111)$ surface, in which Pd has a similar atomic radius to Pt and fully occupied 4d orbitals, the $Pt_3M(111)$ surfaces showed higher oxidative desorption capability than those of the pure Pt(111) surface; electrochemically active surface area recovered at the $Pt_3M(111)$ surfaces by fewer potential cycles than at the Pt(111) surface. Among the various factors, the downshift of the d-band center due to the ligand effect of foreign metal and the electronic interaction between adsorbed S and Pt are the dominant factors promoting the oxidative desorption of sulfur as well as the strain effect of foreign metal with an atomic radius smaller than Pt.

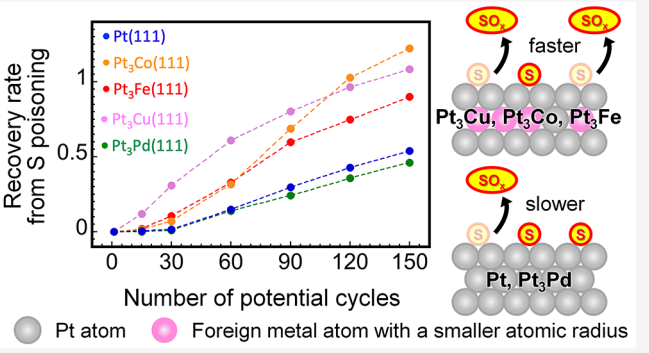

1. INTRODUCTION

Polymer electrolyte membrane fuel cells (PEMFCs) are attracting much attention as clean power sources for transportation applications and residential power systems.[1,2] Sulfur (S) species, which exist in air in volcanic areas and hydrogen fuel gas, are one of the most severe pollutants for PEMFCs.[3] They strongly adsorb on metal surfaces[1,4] including platinum (Pt) surfaces that are most commonly used electrocatalysts in PEMFCs, resulting in the decrease of electrochemically active surface area (ECSA).[1,3,5−7] Therefore, understanding the adsorption/desorption behavior of S species at the Pt-based electrocatalysts is very important to developing electrocatalysts highly tolerant to S poisoning.

The adsorption/desorption of S species at the Pt surface has been extensively studied not only from a fundamental viewpoint[8−13] but also for practical applications in PEMFCs.[5−7,14−21] In conjunction with the development of Clavilier's method[22] and advances in surface characterization techniques[23] since the 1980s, the adsorbed structures of S on various Pt single crystal surfaces were determined on an atomic scale by low energy electron diffraction (LEED)[8−11] and scanning tunneling microscopy (STM).[11−13] Thereafter, the adsorption energy of S on the Pt surfaces was determined by density functional theory (DFT)[4,24−26] based on the experimentally determined atomic arrangement. These studies showed that the adsorption energy depends on the face orientation of the Pt single crystal surfaces and adsorption sites; for example, the adsorption energy of S is higher at the 4-fold hollow site, 3-fold hollow fcc site, hcp site, bridge site, and the atop site in that order.[4,24,26]

Recently, the oxidative desorption behavior of S species at Pt single crystal surfaces has been studied by various electrochemical procedures for a fundamental understanding of S poisoning in PEMFCs.[10,20,27−30] Sung et al. revealed that the current responses characteristic to the S-free bare Pt(111) single crystal surface were substantially blocked by the adsorbed S species, and then those recovered by repeating the electrochemical potential cycling in the range of −0.28 to 0.82 V vs Ag/AgCl because of the oxidative desorption.[10] They also observed the current peak due to the oxidative desorption of S species at 0.7 V vs Ag/AgCl in an aqueous solution of

Received: October 1, 2024
Revised: December 19, 2024
Accepted: December 26, 2024
Published: January 14, 2025

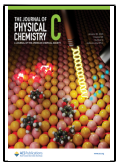

https://doi.org/10.1021/acs.jpcc.4c06652
J. Phys. Chem. C 2025, 129, 2122−2131

sulfuric acid. On the other hand, Chen et al. observed the current peaks due to the oxidative desorption of adsorbed S species from the Pt(111) and Pt(100) surfaces at 1.43 and 1.36 V vs RHE, respectively.[20] They attributed this inconsistency from the previous report by Sung et al.[10] to the different adsorption conditions such as the adsorption potential, concentration, and time. Recently, we further investigated the effect of potential and face orientation on the oxidative desorption behavior of S species using Pt(111), Pt(100), and Pt(110) single-crystal surfaces in an aqueous solution of perchloric acid and revealed that the oxidative desorption of S species occurs at the potential more negative at the Pt(111) surface than at the Pt(110) and Pt(100) surfaces in descending order of adsorption energy of SO_2.[31]

In addition to pure Pt, various Pt-based alloys (denoted as Pt−M), such as Pt−Fe, Pt−Co, and Pt−Ni, have been considered as electrocatalysts in PEMFCs because of their higher catalytic activity toward the oxygen reduction reaction (ORR),[32−37] as well as their impact on cost reduction by reducing the amount of Pt.[38] The origin of their improved catalytic activity for ORR was attributed to the shift of O_2 adsorption energy caused by the downshift of the d-band center of the Pt alloying with foreign metal (M).[39−45] Afterward, the advantages of Pt−M alloys over pure Pt for mitigating the S poisoning were suggested both theoretically[46−49] and experimentally.[16,47−49] Pillay et al.[47] proposed that the adsorption energies of S on the $Pt_3Ni(111)$[46] and $Pt_3Co(111)$ surfaces[47] were lower than those on the Pt(111) surface based on the DFT calculation. In addition, they experimentally demonstrated that the ECSA of the S-adsorbed Pt_3Co nanoparticles recovered by the oxidative desorption after the potential cycling between 0 and 1.03 V vs RHE for 5 times, while that of the S-adsorbed Pt nanoparticles recovered after the same potential cycling for 30 times.[47] Furthermore, Ke et al. reported that the loss of ECSA of the Pt−Co and Pt−Ru nanoparticles during the electrochemical treatments in a sulfur-containing aqueous solution was less severe than that of pure Pt nanoparticles.[48,49] Those alloy nanoparticles also indicated the superior recovery capability from S poisoning to the pure Pt nanoparticles during the potential cycling between 0 and 1.4 V vs RHE probably due to the bifunctional mechanism where CO oxidation was promoted by the adsorbed oxygen on Ru[50] and/or ligand/strain effect of coexisting Co that causes the modulation of electronic state of Pt.[51] Thus, Pt−M alloys are fascinating electrocatalysts in PEMFCs because they can offer not only higher ORR activity and reduced Pt usage but also improved tolerance to S poisoning.

In the present study, we investigated the electrochemical oxidative desorption behavior of S species at the single crystal surfaces of pure Pt and Pt alloying with various foreign metals by repeating the potential cycling between −0.2 and 0.8 V vs Ag/AgCl. According to the discovery in our recent report that Pt(111) surface is most advantageous for recovery from S poisoning among the Pt(111), Pt(110), and Pt(100) surfaces,[31] (111) surfaces of pure Pt and Pt-based alloys were used as working electrodes.

2. METHODS

2.1. Materials. The Pt(111) (10 mm in diameter and 5 mm in thickness) and Pt-based bimetallic alloys denoted as $Pt_3M(111)$ (8 mm in diameter and 2 mm in thickness, atomic ratio of Pt:M = 3:1) single-crystal disks were purchased from Surface Preparation Laboratory and Crystal Base Co., Ltd., respectively. Super special grade $HClO_4$ (60%) and wako special grade Na_2S (98.0%) were purchased from Wako Pure Chemicals. Water was purified by using a Milli-Q system (ELGA LabWater, PURELAB flex3). Ultrapure Ar (99.9995%) and Ar/H_2 mixed gases (95:5 v/v%, 99.999%) were purchased from Suzuki Sho-kan.

2.2. Electrochemical Measurements. The electrode potential was controlled with a potentiostat (Hokuto Denko, HZ-7000). The electrochemical measurements were performed at room temperature using a three-electrode electrochemical cell. A Pt wire and Ag/AgCl electrode (saturated NaCl, +0.200 V vs RHE)[31,52,53] were used as the counter and reference electrodes, respectively. Cyclic voltammetry (CV) measurements were carried out in an Ar-purged 0.1 M $HClO_4$ aqueous electrolyte solution with a scan rate of 50 mV s^{-1}. Hereafter, the potential was expressed with respect to Ag/AgCl unless otherwise specified throughout the paper.

2.3. Sample Preparation. The Pt(111), $Pt_3Fe(111)$, $Pt_3Pd(111)$, $Pt_3Co(111)$, and $Pt_3Cu(111)$ single crystal disks were annealed at 1600, 1400, 1200, 1000, and 1000 °C, respectively, for more than 1 h using an induction heater (Ambrell, EASYHEAT0224) under the flowing Ar/H_2 mixed gas. After cooling under the flowing Ar/H_2 mixed gas, the surfaces of single crystal disks were brought in contact with an Ar-purged 0.1 M $HClO_4$ aqueous electrolyte solution with keeping the potential at 0 V and CVs were measured to ensure the cleanliness and atomic arrangement of the surfaces. This cycle is referred to as precycle in this paper. Then, the disks were immersed in a 1 mM Na_2S aqueous solution under the flowing Ar/H_2 mixed gas for 1 h. After being rinsed with water, the surfaces of the disks were made in contact with a 0.1 M $HClO_4$ aqueous electrolyte solution while keeping the potential at 0 V, and then the electrode potential was cycled between −0.2 and 0.8 V 150 times to quantify the amount of desorbed S from the charge integrations of hydrogen adsorption/desorption waves.

2.4. X-ray photoelectron spectroscopy measurements. X-ray photoelectron spectroscopy (XPS) measurements were carried out using an AXIS-NOVA (Shimadzu/Kratos). All the photoelectron spectra were obtained with a monochromatic Al Kα source ($h\nu$ = 1486.6 eV) at 300 W. The incident angle of the X-rays and the takeoff angle of the photoelectrons were fixed at 35.5 and 90° to the electrode surface, respectively. The pass energy of the electron spectrometer was 80 eV. XPS measurements of Pt(111) and $Pt_3M(111)$ surfaces were performed after induction heating, after immersing in a 1 mM Na_2S aqueous solution, and after electrochemical potential cycling in a 0.1 M $HClO_4$ aqueous electrolyte solution for 15 and 150 times. The samples, except for those after induction heating, were rinsed with water, followed by blowing off the remaining water with air. Then, all of the samples were transferred into the analysis chamber of XPS. The sample transfer was carried out in air and completed in a few minutes. One may be concerned with possible side reactions such as surface oxidation during the sample transfer, but no significant spectral changes were observed in multiple experiments. The intensities of Pt 4f peaks were normalized, and the intensities of S 2p peaks were divided by the integrated intensities of corresponding Pt 4f peaks. Binding energies were calibrated by referencing C 1s peaks that can be assigned to the hydrocarbon contamination (285.0 eV).

https://doi.org/10.1021/acs.jpcc.4c06652
J. Phys. Chem. C 2025, 129, 2122−2131

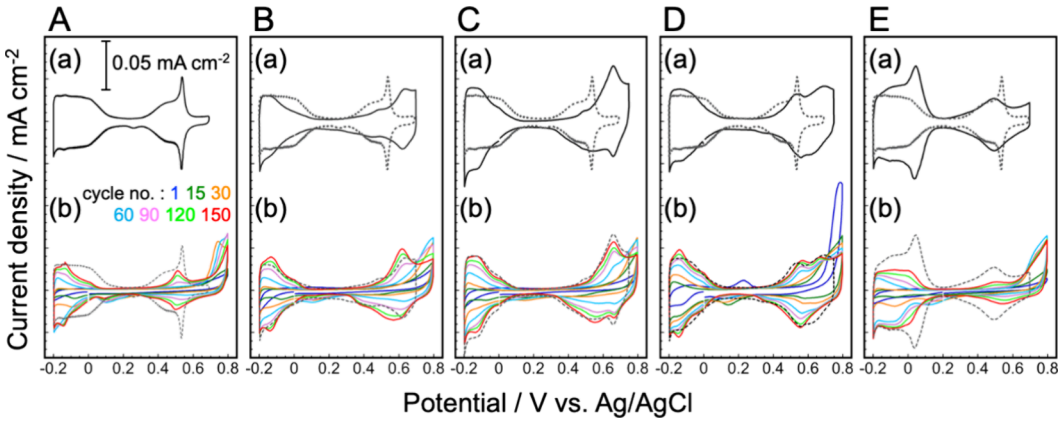

Figure 1. CVs of (a) bare and (b) S-adsorbed (A) Pt(111), (B) Pt_3Co(111), (C) Pt_3Fe(111), (D) Pt_3Cu(111), and (E) Pt_3Pd(111) electrodes measured in a 0.1 M $HClO_4$ aqueous solution with a scan rate of 50 mV s^{-1}. The CV of the bare Pt(111) electrode was shown as a dashed line together with those of bare Pt_3M(111) electrodes. For the CVs of S-adsorbed electrodes, first (blue), 15th (green), 30th (orange), 60th (light blue), 90th (pink), 120th (light green), and 150th cycles (red) were shown.

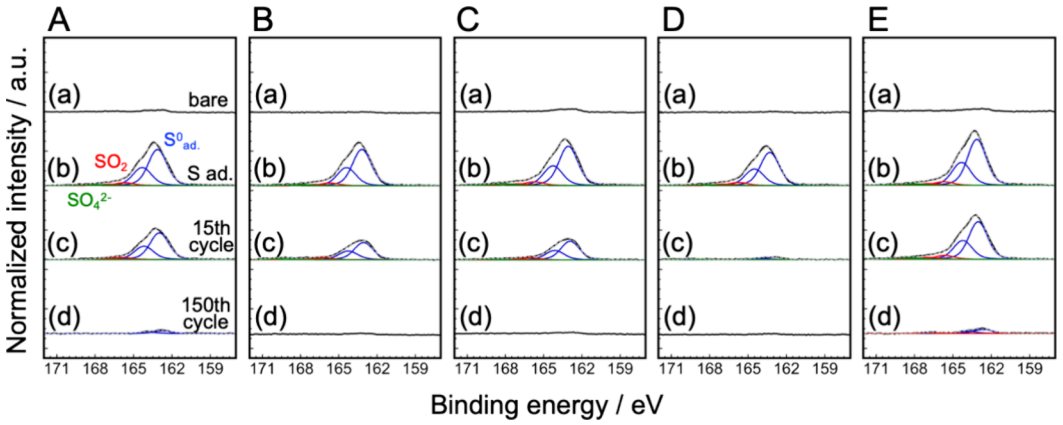

Figure 2. Photoelectron spectra in the S 2p region of (a) bare and S-adsorbed (A) Pt(111), (B) Pt_3Co(111), (C) Pt_3Fe(111), (D) Pt_3Cu(111), and (E) Pt_3Pd(111) electrodes obtained (b) before and after the (c) 15th and (d) 150th potential cycles. The intensity of the S 2p spectra was divided by the integrated intensity of the corresponding Pt 4f spectra.

3. RESULTS AND DISCUSSION

3.1. Pt(111). Figure 1A shows cyclic voltammograms (CVs) of bare and S-adsorbed Pt(111) single crystal electrodes measured in an Ar-purged 0.1 M $HClO_4$ aqueous electrolyte solution with a scan rate of 50 mV s^{-1}. The CV of bare Pt(111) electrode (Figure 1A(a)) shows characteristic current responses such as adsorption/desorption of hydrogen (−0.20 to 0.15 V) and hydroxyl species (0.30 to 0.60 V with a peak at 0.54 V).[54]

After immersing the Pt(111) electrode in a 1 mM Na_2S aqueous solution, those characteristic current responses disappeared (blue line in Figure 1A(b)) and doublet peaks corresponding to adsorbed elemental S (163.1 eV[20,55,56]), as well as indistinct peaks due to SO_2 (165.7 eV[20,55,56]) and SO_4^{2-} (168.0 eV[20,48,55,56]), appeared in the S 2p region of photoelectron spectra (Figure 2A(b)). This suggests that the adsorption/desorption of hydrogen and hydroxyl species was blocked by adsorbed elemental S on the Pt(111) surface. As the number of potential cycles increased, those characteristic current responses gradually recovered and the oxidation current increased at around 0.7 V in the positive going scan (Figure 1A(b)). This oxidation current should be due to the oxidative desorption of adsorbed S, together with the formation of Pt oxide,[31] because the intensities of S 2p peak decreased after the 15th (Figure 2A(c)) and almost disappeared after the 150th potential cycle (Figure 2A(d)). Our recent results suggested that one of the major products of S oxidation is SO_2 at the Pt(111) surface.[31,57] Some SO_2 desorbs from the surface to recover the ECSA, while the remaining SO_2 can be reduced to elemental S adsorbed on Pt in the successive negative going scan. The current waves due to the SO_2 reduction were observed at around 0.1 V and −0.05 V in the negative going scan of the 15th−150th potential cycles (Figure 1A(b)).

In addition, a pair of peaks due to the hydrogen adsorption/desorption at the (110) substep[54] newly appeared at around −0.15 V (Figure 1A(b)) and became larger as the number of potential cycles increased. This indicates that the surface atomic arrangement of Pt(111) changed by repeating oxidation/reduction of Pt.[58−60] CV measurements of S-free bare Pt(111) surface were also performed in a 0.1 M $HClO_4$ aqueous electrolyte solution and a small peak corresponding to the formation of the (110) substep was observed after the potential cycling up to 0.8 V vs Ag/AgCl for 150 times as shown in Figure S1. This suggests that the formation of the (110) substep occurs due to the potential cycling without the oxidative desorption of S. Nevertheless, since the (110) peak in Figure 1A(b) is slightly larger than that in Figure S1, the

https://doi.org/10.1021/acs.jpcc.4c06652
J. Phys. Chem. C 2025, 129, 2122−2131

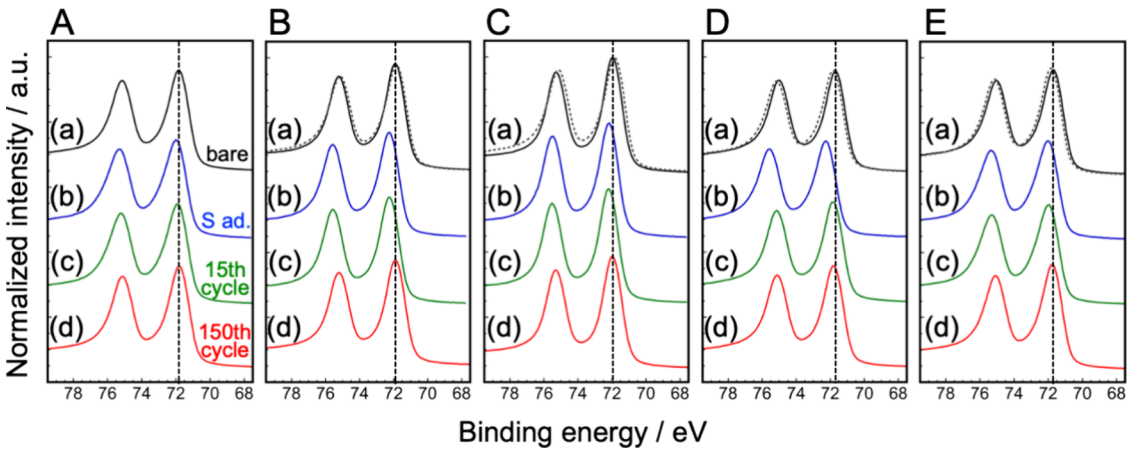

Figure 3. Photoelectron spectra in the Pt 4f region of (a) bare and S-adsorbed (A) Pt(111), (B) $Pt_3Co(111)$, (C) $Pt_3Fe(111)$, (D) $Pt_3Cu(111)$, and (E) $Pt_3Pd(111)$ electrodes obtained (b) before and after the (c) 15th and (d) 150th potential cycles. The spectrum of the bare Pt(111) electrode was shown in dashed line together with those of bare $Pt_3M(111)$ electrodes. All the spectra were normalized so that the integrated peak intensities become constant.

Table 1. Binding Energies (eV) of the Pt $4f_{7/2}$ Peaks of Bare and S-Adsorbed Pt(111), $Pt_3Co(111)$, $Pt_3Fe(111)$, $Pt_3Cu(111)$, and $Pt_3Pd(111)$ Electrodes Obtained before and after the 15th and 150th Potential Cycles

	Pt(111)	$Pt_3Co(111)$	$Pt_3Fe(111)$	$Pt_3Cu(111)$	$Pt_3Pd(111)$
bare	71.8	71.9	71.9	71.7	71.6
S-adsorbed (before potential cycling)	71.9	72.2	72.1	72.2	71.9
after 15th cycle	71.9	72.2	72.2	71.8	71.9
after 150th cycle	71.8	71.9	71.9	71.7	71.7

formation of the (110) site can be accelerated by the oxidation desorption of S.

Figure 3A shows Pt 4f photoelectron spectra of the S-adsorbed Pt(111) surfaces before and after the potential cycles together with that of the bare Pt(111) surface as a reference. The binding energies of the Pt $4f_{7/2}$ peaks were summarized in Table 1. At the S-adsorbed Pt(111) surface (Figure 3A(b), (c)), Pt 4f peaks shifted by 0.1 eV to a higher binding energy as compared to that of the bare Pt(111) surface (Figure 3A(a)). After the desorption of S species (Figure 3A(d)), however, the Pt 4f peak reverted to the original position, the same as that of the bare Pt(111) surface (Figure 3A(a)). The shift of Pt 4f peaks is similar to but smaller than that reported for the Pt black catalyst where S is adsorbed with weak Pt−S electronic interaction.[56] These results suggest the electronic interaction between adsorbed S and Pt at the S-adsorbed Pt(111) surface as is the case of CO adsorbed Pt surface.[51]

3.2. $Pt_3Co(111)$ and $Pt_3Fe(111)$. Figure 1B,C shows CVs of bare and S-adsorbed $Pt_3Co(111)$ and $Pt_3Fe(111)$ single crystal electrodes measured in an Ar-purged 0.1 M $HClO_4$ aqueous electrolyte solution with a scan rate of 50 mV s^{-1}. The CVs of bare $Pt_3Co(111)$ (solid line in Figure 1B(a)) and $Pt_3Fe(111)$ electrodes (solid line in Figure 1C(a)) were different from that of pure Pt(111) electrode (solid line in Figure 1A(a) and dashed lines in Figure 1B(a),C(a)) but in accordance with the CVs of previous report for $Pt_3Co(111)$ and $Pt_3Fe(111)$ electrodes covered with a Pt skin layer.[61,62] The positive potential end of hydrogen adsorption/desorption waves became narrower than that of the Pt(111) electrode (Figure 1B(a),C(a)). In addition, the hydroxyl adsorption/desorption peaks split into two components; a very small shoulder peak at around 0.5 V that is almost the same potential as the hydroxyl adsorption/desorption peak at the Pt(111) electrode and a positively shifted broad peak at around 0.6 V (Figure 1B(a),C(a)). Thus, the outermost layer of $Pt_3Co(111)$ and $Pt_3Fe(111)$ electrodes after induction heating in the present study is considered to be a Pt skin layer as previously demonstrated,[61,62] resulting from the Pt surface segregation.[63,64]

After immersing the Pt skin-covered $Pt_3Co(111)$ and $Pt_3Fe(111)$ electrodes in a 1 mM Na_2S aqueous solution, the characteristic current responses disappeared (blue lines in Figure 1B(b),C(b)) and a pair of peaks corresponding to elemental S (163.2 eV[20,55,56]), as well as indistinct peaks due to SO_2 (165.8 eV[20,55,56]) and SO_4^{2-} (168.1 eV[20,48,55,56]), appeared in the S 2p region of photoelectron spectra (Figure 2B(b) and Figure 2C(b)), showing the blocking of adsorption/desorption of hydrogen and hydroxyl species by the adsorbed S species. As the number of potential cycles increased, those missing current responses gradually recovered (Figure 1B-B(b),C(b)). Simultaneously, the current attributable to the oxidation of adsorbed S species at around 0.7 V increased for both electrodes (Figure 1B(b) and Figure 1C(b)). The intensities of S 2p peaks significantly decreased after the 15th potential cycle (Figure 2B(c),C(c)) and almost completely disappeared after the 150th potential cycle (Figure 2B(d),C(d)). The intensities of S 2p peaks at the S-adsorbed $Pt_3Co(111)$ and $Pt_3Fe(111)$ surfaces were similar to each other under the same potential cycling conditions but substantially smaller than those of the Pt(111) surface (Figure 2A(d)), implying the acceleration of oxidative desorption of S by alloying with Co and Fe.

In the case of $Pt_3Co(111)$, a pair of reversible peaks assignable to the hydrogen adsorption/desorption at the (110) substep[54] appeared at around −0.15 V and became larger as the number of potential cycles increased (Figure 1B(b)), indicating that the surface atomic arrangement of Pt-skinned $Pt_3Co(111)$ electrode changed during the potential cycling. In

https://doi.org/10.1021/acs.jpcc.4c06652
J. Phys. Chem. C 2025, 129, 2122−2131

contrast, unlike the Pt(111) and Pt_3Co(111) electrodes (Figure 1A(b),B(b)), the reversible peaks corresponding to the hydrogen adsorption/desorption at the (110) substep were absent at the Pt_3Fe(111) electrode after the 150th potential cycle (Figure 1C(b)), indicating that the surface atomic arrangement of Pt-skinned Pt_3Fe(111) electrode was maintained during the potential cycles in this potential range. Since the surface roughening often produces low coordination Pt atoms that are less stable for dissolution as evidenced both experimentally and theoretically,[65−67] the Pt_3Fe(111) electrode with less surface roughening is potentially more tolerant to the adsorption/desorption of S and/or oxidation/reduction of Pt/Pt oxide by potential cycling.

Figure 3B,C shows the Pt 4f photoelectron spectra of the S-adsorbed Pt_3Co(111) and Pt_3Fe(111) surfaces before and after potential cycles together with those of bare Pt_3Co(111) and Pt_3Fe(111) surfaces as a reference. Consistent with the previous reports,[48,51] the binding energies of the Pt 4f peak of bare Pt_3Co(111) and Pt_3Fe(111) surfaces were higher than that of bare Pt(111) surface (Figure 3B(a),C(a) and Table 1), indicating that the electronic state of surface Pt atoms was modulated by alloying with Co and Fe due to the lattice strain (strain effect) and electronic interaction (ligand effect).[45,64,68−70] Yu et al. calculated the d-band center of the surface layer of the surface segregated Pt_3M alloys, where M is any of the three rows of transition metals (columns 3−12).[64] Ou et al. also calculated the d-band center for the Pt-segregated surface of various Pt_3M alloys, where M is almost the same as those reported by Yu et al.[64] but except for Tc, Os, and Hg, and concluded that for 3d transition metals except for Sc and Cu, both strain and ligand effects cause downshift of the d-band center of Pt-segregated surface.[70] Note that both studies show close values for the d-band center in each alloy, albeit with slight differences. Thus, the shift of Pt 4f peak to a higher binding energy, observed for Pt_3Co(111) and Pt_3Fe(111), is considered to be brought about by the downshift of the d-band center away from the Fermi level.[51]

At the S-adsorbed Pt_3Co(111) and Pt_3Fe(111) surfaces (Figure 3B(b),C(b)), the Pt 4f peak shifted by 0.3 and 0.2 eV to a higher binding energy than that at the bare Pt_3Co(111) and Pt_3Fe(111) surfaces (Figure 3B(a),C(a) and Table 1), respectively, suggesting the electronic interaction between adsorbed S and Pt at the S-adsorbed electrodes as described in the preceding section (3.1). Whereas the peak position remained unchanged in the photoelectron spectra after the 15th potential cycle (Figure 3B(c),C(c) and Table 1), it reverted to the original position same as those of bare Pt_3Co(111) and Pt_3Fe(111) surfaces after the 150th potential cycle (Figure 3B(d),C(d) and Table 1) where the S species completely desorbed from the surface as evident by photoelectron spectra in S 2p region (Figure 2B(d),C(d)). This confirms the occurrence of electronic interaction between adsorbed S and Pt at the S-adsorbed Pt_3Co(111) and Pt_3Fe(111) surfaces. Thus, the trends of electrochemical responses and spectral features at the bare and S-adsorbed Pt_3Co(111) and Pt_3Fe(111) electrodes were similar to each other, except for the potentially higher tolerance of Pt_3Fe(111) electrode to the surface roughening by potential cycling.

3.3. Pt_3Cu(111) and Pt_3Pd(111). Figure 1D,E shows CVs of bare and S-adsorbed Pt_3Cu(111) and Pt_3Pd(111) single crystal electrodes measured in an Ar-purged 0.1 M $HClO_4$ aqueous electrolyte solution with a scan rate of 50 mV s^{-1}. The CV of bare Pt_3Cu(111) electrode (Figure 1D(a)) exhibited similar characteristics to those of Pt_3Co(111) and Pt_3Fe(111) electrodes (Figure 1B(a) and Figure 1C(a)) in the following aspects; the hydrogen adsorption/desorption waves were distorted and the hydroxyl adsorption/desorption peaks split into the two broad components. However, it is worth noting here, with respect to Pt_3Cu(111) that there are two notable differences from Pt_3Co(111) and Pt_3Fe(111). Whereas the shoulder peaks at around 0.5 V were much smaller than the positively shifted peaks at 0.6 V at the Pt_3Co(111) and Pt_3Fe(111) electrodes (Figure 1B(a),C(a)), the peak at around 0.5 V was comparable to positively shifted ones (Figure 1D(a)). In addition, the positively shifted peak was observed at around 0.7 V (Figure 1D(a)), which is 0.1 V more positive than those at the Pt_3Co(111) and Pt_3Fe(111) electrodes (Figure 1B(a),C(a)). Notably, theoretical calculations predicted that a Pt surface segregation in Pt_3Cu(111) is either weak[63] or possible but not strong,[64,70] and for Pt−Cu alloys, both experimental and theoretical studies suggested that the Pt segregation tends not to be so obvious and varies with conditions.[71−73] Jensen et al. reported that the positive potential shift of the adsorption/desorption peaks of hydroxyl species became larger as increasing the Cu content at the Cu/Pt(111) near-surface alloy.[72] They also reported that the hydroxyl adsorption/desorption peaks reached 0.69 V when a Pt skin layer was formed on a complete monatomic Cu second layer. Thus, the surface of the Pt_3Cu(111) electrode in the present study was probably covered by the Pt skin outermost layer formed on the Cu second layer but partially phase-separated.

The CV of the bare Pt_3Pd(111) electrode (solid line of Figure 1E(a)) was distinctively different not only from that of the pure Pt(111) electrode (solid line of Figure 1A(a) and dashed line of Figure 1E(a)) but also from those of any other Pt_3M(111) electrodes examined in this study (solid lines of Figure 1B−D(a)); a new reversible peak appeared at around 0.05 V and the hydroxyl adsorption/desorption peaks became broader and shifted to negative potential as compared to the CV of the Pt(111) electrode (solid line of Figure 1A(a) and dashed line of Figure 1E(a)). Also notably here, theoretical calculations predicted little Pt segregation on the surfaces of Pt_3Pd(111),[63,64,70] and both experimental and theoretical studies indicated that no preferred surface segregation of Pt occurs in Pt−Pd alloys, but rather that Pd would enrich the outermost layer of alloys.[73−75] The characteristics of CV observed for bare Pt_3Pd(111) electrode imply that hydrogen and hydroxyl species adsorb on the Pt_3Pd(111) electrode more strongly than on the Pt(111) electrode[76] probably due to the upshift of d-band center.[64,70,77]

After immersing the Pt_3Cu(111) and Pt_3Pd(111) electrodes in a 1 mM Na_2S aqueous solution, those characteristic current responses disappeared (blue lines in Figure 1D(b) and Figure 1E(b)) and doublet peaks corresponding to adsorbed elemental S (163.3 eV[20,55,56]) and very small peaks due to SO_2 (165.7 eV[20,55,56]) and SO_4^{2-} (168.4 eV[20,48,55,56]) appeared in the S 2p region of photoelectron spectra (Figure 2D(b) and Figure 2E(b)). One may be concerned with the formation of CuS at the Pt_3Cu(111) surface, but the position of the S 2p peak of the S-adsorbed Pt_3Cu(111) surface was totally different from that of CuS deposited on a polycrystalline Pt surface as shown in Figure S2 and previous report.[78] The intensity of the S 2p peak at the S-adsorbed Pt_3Cu(111) surface shown in Figure 2D(b) is slightly smaller than those of

https://doi.org/10.1021/acs.jpcc.4c06652
J. Phys. Chem. C 2025, 129, 2122−2131

the other surfaces, implying its potentially high tolerance to S adsorption.

Interestingly, in addition to a small current peak at around 0.2 V, oxidation current significantly larger than those of the other electrodes (blue lines in Figure 1A−C,E(b)) started to be observed from around 0.6 V only in the first potential cycle of the S-adsorbed $Pt_3Cu(111)$ electrode (blue line in Figure 1D(b)). The small current peak can be attributed to the dissolution of Cu from the phase-separated Cu domain because the potential is in reasonable agreement with the redox potential of Cu, originally reported as 0.342 V vs SHE.[79] This small oxidation peak was not observed at the bare $Pt_3Cu(111)$ surface but only after the S adsorption, suggesting that the dissolution of phase-separated Cu was accelerated by adsorbed S species as previously reported.[80,81] The large oxidation current rising from 0.6 V should be due to the oxidation of adsorbed S because the current wave corresponding to the reduction of SO_2 at around −0.1 V in the successive negative going scan of the first potential cycle (blue line in Figure 1D(b))[31] was also larger than those of the other electrodes (blue lines in Figure 1A−C,E(b)). Moreover, the S 2p peak of the S-adsorbed $Pt_3Cu(111)$ surface almost disappeared after the 15th potential cycle (Figure 2D(c)) although the S 2p peaks were still present at the surfaces of other electrodes at this stage (Figure 2A−C,E(c)), indicating that the oxidative desorption of S at the $Pt_3Cu(111)$ surface is faster than the others. By repeating the potential cycles, the hydrogen and hydroxyl adsorption/desorption current waves recovered gradually and almost reverted to the original shapes characteristic of the bare $Pt_3Cu(111)$ electrode after the 90th potential cycle (pink line in Figure 1D(b)). This confirms that despite the dissolution of phase-separated Cu, the atomic arrangement of the $Pt_3Cu(111)$ electrode was almost maintained.

As the number of potential cycles increased at the S-adsorbed $Pt_3Pd(111)$ electrode, the hydrogen adsorption/desorption waves gradually recovered (Figure 1E(b)). However, the intensity of the S 2p peak after the 15th potential cycle (Figure 2E(c)) was much larger than those of Pt(111) and other $Pt_3M(111)$ electrodes (Figure 2A−D(c)), suggesting that the oxidative desorption of S at the $Pt_3Pd(111)$ electrode is slower than the others. Even after the 150th potential cycle where the hydrogen adsorption/desorption waves almost completely recovered at the other $Pt_3M(111)$ electrodes (dashed lines and red lines in Figure 1B−D(b)), it recovered only up to 46% of that of the original bare $Pt_3Pd(111)$ electrode (dashed line and red line in Figure 1E(b)). In addition, the reversible peak observed at around 0.05 V, which is characteristic to the bare $Pt_3Pd(111)$ electrode (solid line in Figure 1E(a) and dashed line in Figure 1E(b)) was missing and the shape of CV (red line in Figure 1E(b)) resembles that of bare pure Pt(111) electrode (Figure 1A(a) and dashed line in Figure 1E(a)). These characteristics are probably due to the enhancement of S adsorption by the presence of Pd in the outermost layer.[82]

Figure 3D,E shows Pt 4f photoelectron spectra of the S-adsorbed $Pt_3Cu(111)$ and $Pt_3Pd(111)$ surfaces before and after the potential cycles together with those of bare $Pt_3Cu(111)$ and $Pt_3Pd(111)$ surfaces as a reference. In contrast to the $Pt_3Co(111)$ and $Pt_3Fe(111)$ surfaces, the binding energies of Pt 4f peak of bare $Pt_3Cu(111)$ and $Pt_3Pd(111)$ surfaces were lower by 0.1 and 0.2 eV than that of bare Pt(111) surface (Figure 3D(a),E(a) and Table 1). This is consistent with the previous reports at the $Pt_3Pd(111)$ surface.[83,84]

The ligand effect of transition metals was reported to generally cause a downshift of the d-band center of Pt-segregated surface in most Pt_3M alloys, except for those in which M has fully occupied the outermost d orbitals.[70] Although Cu has fully occupied 3d orbitals that bring about the upshift of the d-band center, its smaller atomic radius causes the downshift and, as a result, ligand and strain effects of Cu are nearly canceled out.[70] On the other hand, since Pd has fully occupied 4d orbitals and an atomic radius similar to Pt, the ligand effect is more dominant, leading to the upshift of the d-band center toward the Fermi level.[70] Thus, the shift of the Pt 4f peak to a lower binding energy at the $Pt_3Pd(111)$ electrode is more prominent than that of the $Pt_3Cu(111)$ electrode.

At the S-adsorbed $Pt_3Cu(111)$ and $Pt_3Pd(111)$ surfaces (Figure 3D(b) and Figure 3E(b)), the Pt 4f peaks shifted by 0.5 and 0.3 eV to a higher binding energy than those of bare $Pt_3Cu(111)$ and $Pt_3Pd(111)$ surfaces (Figure 3D(a),E(a) and Table 1), respectively, presumably due to the electronic interaction between adsorbed S and Pt. The Pt 4f peak of the S-adsorbed $Pt_3Cu(111)$ surface shifted to a lower binding energy after the 15th potential cycle (Figure 3D(c) and Table 1) where the S 2p peak almost disappeared, and completely recovered to the original position of bare $Pt_3Cu(111)$ surface after 150th potential cycle (Figure 3D(d) and Table 1). In the case of the S-adsorbed $Pt_3Pd(111)$ surface, however, the position of the Pt 4f peak remained almost unchanged after the 15th potential cycle (Figure 3E(c) and Table 1) and it was still higher by 0.1 eV than that of the bare $Pt_3Pd(111)$ surface even after the 150th potential cycle (Figure 3E(d) and Table 1). Thus, we confirmed the electronic interaction between adsorbed S and Pt at the S-adsorbed Pt(111) and all of the $Pt_3M(111)$ surfaces.

3.4. Recovery Rate. To elucidate the effect of alloying on the oxidative desorption of S species, the recovery factor, RF is defined as eq 1 based on the electrochemical charge integrations of hydrogen desorption current at the Pt(111) and $Pt_3M(111)$ electrodes.

$$\mathrm{RF} = \frac{C_{\mathrm{S-adsorbed}}}{C_{\mathrm{bare}}} \tag{1}$$

where $C_{\mathrm{S\text{-}adsorbed}}$ and C_{bare} are the charge integrations of hydrogen desorption waves at the S-adsorbed electrodes after potential cycling and bare electrodes, respectively. Figure 4 shows the plot of RF with respect to the number of potential cycles.

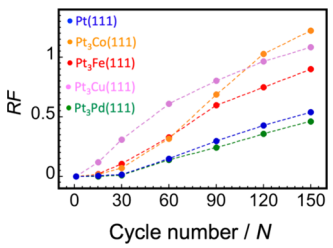

Figure 4. Recovery factor, RF, of the S-adsorbed Pt(111), $Pt_3Co(111)$, $Pt_3Fe(111)$, $Pt_3Cu(111)$, and $Pt_3Pd(111)$ electrodes against the number of potential cycles.

https://doi.org/10.1021/acs.jpcc.4c06652
J. Phys. Chem. C 2025, 129, 2122−2131

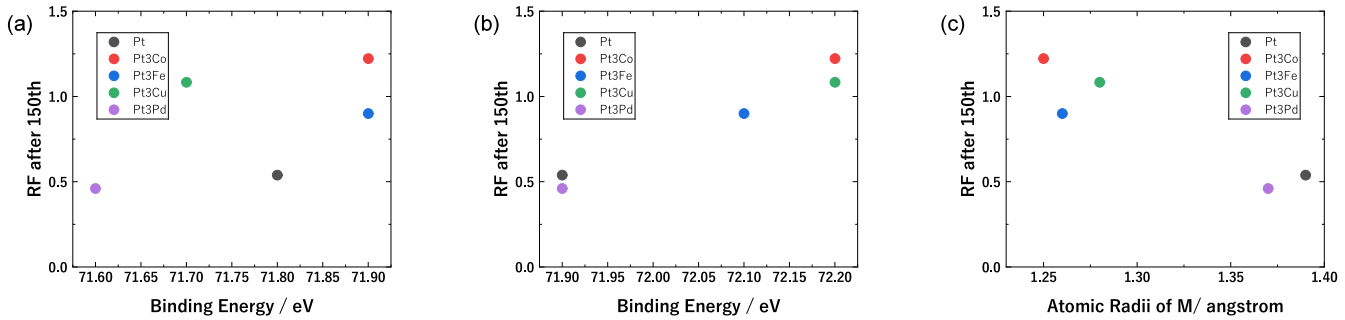

Figure 5. RFs after 150th potential cycles with respect to the binding energy of Pt 4f peaks of Pt(111), Pt_3Co(111), Pt_3Fe(111), Pt_3Cu(111), and Pt_3Pd(111) electrodes (a) before and (b) after the adsorption of S species and (c) atomic radii of Pt for the Pt(111) electrode and foreign metal M (Co, Fe, Cu, Pd) for Pt_3M(111) electrodes.

RFs were higher at the Pt_3Cu(111), Pt_3Co(111), Pt_3Fe-(111), Pt(111), and Pt_3Pd(111) electrodes in that order up to the 90th cycle, and the RF of the Pt_3Co(111) electrode became higher than that of the Pt_3Cu(111) electrode from the 120th cycle. Except for the Pt_3Pd(111) electrode, RFs of the Pt_3M(111) electrodes were higher than those of the Pt(111) electrode. It is noted that RFs of the Pt_3Co(111) electrode at the 120th and 150th cycles became larger than 1, due to the surface roughening caused by the oxidation/reduction cycles.

Ligand effect and strain effect are considered as the dominant factors for RFs and thus RFs after 150th potential cycles were plotted with respect to the binding energies of Pt 4f peaks of Pt(111) and Pt_3M(111) electrodes before and after the adsorption of S species and atomic radii of Pt and foreign metal M (Figure 5). Whereas the correlation between RF and binding energy of the Pt 4f peak of bare Pt(111) and Pt_3M(111) electrodes was unclear (Figure 5(a)), RF monotonically increased as the Pt 4f peaks of S-adsorbed Pt(111) and Pt_3M(111) electrodes became higher (Figure 5(b)). This result suggests that the electronic structure of S-adsorbed Pt(111) and Pt_3M(111) electrodes is one of the important factors because the shift of the Pt 4f peak to a higher binding energy represents the downshift of the d-band center away from the Fermi level as discussed in the sections above. Thus, the downshift of the d-band center caused by both the ligand effect of foreign metal M and electronic interaction between adsorbed S and Pt atoms substantially accelerates the electrochemical oxidative desorption of S species. In addition, RF became higher as the atomic radii of foreign metal M became smaller (Figure 5(c)). The difference in atomic radii of Pt and foreign metal M is the measure of another important factor, the strain effect. The strain introduced by alloying Pt with a foreign metal with a smaller atomic radius also promotes the oxidative desorption of the S species.

4. CONCLUSIONS

We investigated the oxidative desorption behavior of S species on the Pt(111), Pt_3Co(111), Pt_3Fe(111), Pt_3Cu(111), and Pt_3Pd(111) electrodes by electrochemical measurements and XPS. We confirmed that the adsorption and desorption of hydrogen and hydroxyl species were blocked by adsorbed S species on the electrode surfaces. However, the adsorbed S species oxidatively desorbed from the electrode surfaces by the potential cycling. The oxidative desorption of S species, i.e., recovery from the S poisoning was slower at the Pt_3Pd(111) electrode than at the Pt(111) electrode, whereas it was faster at the Pt_3Cu(111), Pt_3Co(111) and Pt_3Fe(111) electrodes than at the Pt(111) electrode in that order. This trend was ruled by the downshift of the d-band center due to the ligand effect of foreign metal and electronic interaction between adsorbed S and Pt, as well as the strain effect. Thus, the S oxidative desorption capability of Pt electrocatalysts can be improved by alloying with foreign metals, especially with a smaller atomic radius.

■ ASSOCIATED CONTENT

Supporting Information

The Supporting Information is available free of charge at https://pubs.acs.org/doi/10.1021/acs.jpcc.4c06652.

Potential cycling experiment for S-free bare Pt(111) electrode; XPS measurements of Pt_3Cu(111) surface and CuS deposited on polycrystalline Pt surface (PDF)

■ AUTHOR INFORMATION

Corresponding Author

Takuya Masuda − *Research Center for Energy and Environmental Materials (GREEN), National Institute for Materials Science (NIMS), Tsukuba, Ibaraki 305-0044, Japan; Graduate School of Chemical Sciences and Engineering, Hokkaido University, Sapporo, Hokkaido 060-0810, Japan;* orcid.org/0000-0001-7462-2177; Email: MASUDA.Takuya@nims.go.jp

Authors

Makoto Aoki − *Research Center for Energy and Environmental Materials (GREEN), National Institute for Materials Science (NIMS), Tsukuba, Ibaraki 305-0044, Japan;* Present Address: Toyota Boshoku Corporation, Kariya, Aichi 448-8651, Japan

Tamao Shishido − *Research Center for Energy and Environmental Materials (GREEN), National Institute for Materials Science (NIMS), Tsukuba, Ibaraki 305-0044, Japan*

Tetsuro Morooka − *Research Center for Energy and Environmental Materials (GREEN), National Institute for Materials Science (NIMS), Tsukuba, Ibaraki 305-0044, Japan*

Takuya Nakanishi − *Research Center for Energy and Environmental Materials (GREEN), National Institute for Materials Science (NIMS), Tsukuba, Ibaraki 305-0044, Japan;* orcid.org/0000-0002-1172-718X

Complete contact information is available at: https://pubs.acs.org/10.1021/acs.jpcc.4c06652

https://doi.org/10.1021/acs.jpcc.4c06652
J. Phys. Chem. C 2025, 129, 2122−2131

Notes

The authors declare no competing financial interest.

■ ACKNOWLEDGMENTS

This paper is based on results obtained from a project, JPNP20003, commissioned by the New Energy and Industrial Technology Development Organization (NEDO).

■ REFERENCES

(1) Borup, R.; Meyers, J.; Pivovar, B.; Kim, Y. S.; Mukundan, R.; Garland, N.; Myers, D.; Wilson, M.; Garzon, F.; Wood, D.; et al. Scientific Aspects of Polymer Electrolyte Fuel Cell Durability and Degradation. *Chem. Rev.* **2007**, *107* (10), 3904−3951.
(2) Mancino, A. N.; Menale, C.; Vellucci, F.; Pasquali, M.; Bubbico, R. PEM Fuel Cell Applications in Road Transport. *Energies* **2023**, *16* (17), 6129.
(3) Moore, J. M.; Adcock, P. L.; Lakeman, J. B.; Mepsted, G. O. The effects of battlefield contaminants on PEMFC performance. *J. Power Sources* **2000**, *85* (2), 254−260.
(4) Bernard Rodríguez, C. R.; Santana, J. A. Adsorption and diffusion of sulfur on the (111), (100), (110), and (211) surfaces of FCC metals: Density functional theory calculations. *J. Chem. Phys.* **2018**, *149* (20), No. 204701.
(5) Mohtadi, R.; Lee, W. K.; Van Zee, J. W. The effect of temperature on the adsorption rate of hydrogen sulfide on Pt anodes in a PEMFC. *Applied Catalysis B: Environmental* **2005**, *56* (1), 37−42.
(6) Nagahara, Y.; Sugawara, S.; Shinohara, K. The impact of air contaminants on PEMFC performance and durability. *J. Power Sources* **2008**, *182* (2), 422−428.
(7) Gould, B. D.; Baturina, O. A.; Swider-Lyons, K. E. Deactivation of Pt/VC proton exchange membrane fuel cell cathodes by SO_2, H_2S and COS. *J. Power Sources* **2009**, *188* (1), 89−95.
(8) Marcus, P.; Protopopoff, E. Coadsorption of sulphur and hydrogen on platinum (110) studied by radiotracer and electrochemical techniques. *Surf. Sci.* **1985**, *161* (2), 533−552.
(9) Batina, N.; McCargar, J. W.; Salaita, G. N.; Lu, F.; Laguren-Davidson, L.; Lin, C. H.; Hubbard, A. T. Structure and composition of platinum(111) and platinum(100) surfaces as a function of electrode potential in aqueous sulfide solutions. *Langmuir* **1989**, *5* (1), 123−128.
(10) Sung, Y. E.; Chrzanowski, W.; Zolfaghari, A.; Jerkiewicz, G.; Wieckowski, A. Structure of Chemisorbed Sulfur on a Pt(111) Electrode. *J. Am. Chem. Soc.* **1997**, *119* (1), 194−200.
(11) Yoon, H. A.; Materer, N.; Salmeron, M.; Van Hove, M. A.; Somorjai, G. A. Coverage-dependent structures of sulfur on Pt(111) studied by low-energy electron diffraction (LEED) and scanning tunneling microscopy (STM). *Surf. Sci.* **1997**, *376* (1), 254−266.
(12) Maurice, V.; Marcus, P. STM imaging in air with atomic resolution of adsorbates on metal surfaces: Pt(100)-c(2 × 2)s. *Surf. Sci.* **1992**, *262* (1), L59−L64.
(13) McIntyre, B. J.; Sautet, P.; Dunphy, J. C.; Salmeron, M.; Somorjai, G. A. Scanning tunneling microscopy tip-dependent image contrast of S/Pt(111) by controlled atom transfer*. *Journal of Vacuum Science & Technology B: Microelectronics and Nanometer Structures Processing, Measurement, and Phenomena* **1994**, *12* (3), 1751−1753.
(14) Shi, W.; Yi, B.; Hou, M.; Jing, F.; Ming, P. Hydrogen sulfide poisoning and recovery of PEMFC Pt-anodes. *J. Power Sources* **2007**, *165* (2), 814−818.
(15) Fu, J.; Hou, M.; Du, C.; Shao, Z.; Yi, B. Potential dependence of sulfur dioxide poisoning and oxidation at the cathode of proton exchange membrane fuel cells. *J. Power Sources* **2009**, *187* (1), 32−38.
(16) Ramaker, D. E.; Gatewood, D.; Korovina, A.; Garsany, Y.; Swider-Lyons, K. E. Resolving Sulfur Oxidation and Removal from Pt and Pt_3Co Electrocatalysts Using in Situ X-ray Absorption Spectroscopy. *J. Phys. Chem. C* **2010**, *114* (27), 11886−11897.
(17) Park, I.-S.; Xu, B.; Atienza, D. O.; Hofstead-Duffy, A. M.; Allison, T. C.; Tong, Y. J. Chemical State of Adsorbed Sulfur on Pt Nanoparticles. *ChemPhysChem* **2011**, *12* (4), 747−752.
(18) Awad, M. I.; Saleh, M. M.; Ohsaka, T. Electroactivity regeneration of sulfur-poisoned platinum nanoparticle-modified glassy carbon electrode at low anodic potentials. *J. Solid State Electrochem.* **2015**, *19* (5), 1331−1340.
(19) Potgieter, M.; Parrondo, J.; Ramani, V. K.; Kriek, R. J. Evaluation of Polycrystalline Platinum and Rhodium Surfaces for the Electro-Oxidation of Aqueous Sulfur Dioxide. *Electrocatalysis* **2016**, *7* (1), 50−59.
(20) Chen, C.-H.; Halford, A.; Walker, M.; Brennan, C.; Lai, S. C. S.; Fermin, D. J.; Unwin, P. R.; Rodriguez, P. Electrochemical characterization and regeneration of sulfur poisoned Pt catalysts in aqueous media. *J. Electroanal. Chem.* **2018**, *816*, 138−148.
(21) Ke, S.; Sun, C.; Cui, B.; Qin, Y.; Dou, M. Operatable and Efficient Mitigation Strategies for H2S Poisoning in Proton Exchange Membrane Fuel Cells: Releasing Pt Reactive Sites for Hydrogen Oxidation. *ACS Applied Energy Materials* **2023**, *6* (6), 3337−3346.
(22) Clavilier, J.; Faure, R.; Guinet, G.; Durand, R. Preparation of monocrystalline Pt microelectrodes and electrochemical study of the plane surfaces cut in the direction of the {111} and {110} planes. *Journal of Electroanalytical Chemistry and Interfacial Electrochemistry* **1980**, *107* (1), 205−209.
(23) Masuda, T.; Uosaki, K., Novel In Situ Techniques. In *Electrochemical Science for a Sustainable Society: A Tribute to John O'M Bockris*, Uosaki, K., Ed. Springer International Publishing: Cham, 2017; pp 147−174.
(24) Alfonso, D. R. Computational Studies of Experimentally Observed Structures of Sulfur on Metal Surfaces. *J. Phys. Chem. C* **2011**, *115* (34), 17077−17091.
(25) Ungerer, M. J.; Santos-Carballal, D.; Cadi-Essadek, A.; van Sittert, C. G. C. E.; de Leeuw, N. H. Interaction of SO_2 with the Platinum (001), (011), and (111) Surfaces: A DFT Study. *Catalysts* **2020**, *10* (5), 558.
(26) Ungerer, M. J.; van Sittert, C. G. C. E.; de Leeuw, N. H. Behavior of S, SO, and SO_3 on Pt (001), (011), and (111) surfaces: A DFT study. *J. Chem. Phys.* **2021**, *154* (19), No. 194701.
(27) Quijada, C.; Vázquez, J. L.; Pérez, J. M.; Aldaz, A. Voltammetric behaviour of irreversibly adsorbed SO_2 on a Pt(111) electrode in sulphuric acid medium. *J. Electroanal. Chem.* **1994**, *372* (1), 243−250.
(28) Sung, Y. E.; Chrzanowski, W.; Wieckowski, A.; Zolfaghari, A.; Blais, S.; Jerkiewicz, G. Coverage evolution of sulfur on Pt(111) electrodes: From compressed overlayers to well-defined islands. *Electrochim. Acta* **1998**, *44* (6), 1019−1030.
(29) Dourado, A. H. B.; Colle, V. D.; Munhos, R. L.; Feliu, J. M.; Varela, H.; de Torresi, S. I. C. SO_2 electrooxidation reaction on Pt single crystal surfaces in acidic media: Electrochemical and in situ FTIR studies. *Electrochim. Acta* **2022**, *403*, No. 139601.
(30) Kattwinkel, L.; Magnussen, O. M. Optical reflectance studies on the oxidation of chemisorbed sulfur at the Pt(111) electrode. *Electrochim. Acta* **2022**, *434*, No. 141297.
(31) Morooka, T.; Shishido, T.; Devivaraprasad, R.; Elumalai, G.; Aoki, M.; Shirasawa, T.; Nakanishi, T.; Ishikawa, A.; Kondo, T.; Masuda, T. Potential-Dependent and Face Orientation-Dependent Electrochemical Oxidative Desorption Behavior of Sulfur Species Adsorbed on Platinum Single-Crystal Surfaces. *J. Phys. Chem. C* **2024**, *128*, 16426−16436.
(32) Mukerjee, S.; Srinivasan, S. Enhanced electrocatalysis of oxygen reduction on platinum alloys in proton exchange membrane fuel cells. *J. Electroanal. Chem.* **1993**, *357* (1), 201−224.
(33) Toda, T.; Igarashi, H.; Uchida, H.; Watanabe, M. Enhancement of the Electroreduction of Oxygen on Pt Alloys with Fe, Ni, and Co. *J. Electrochem. Soc.* **1999**, *146* (10), 3750.
(34) Min, M.-k.; Cho, J.; Cho, K.; Kim, H. Particle size and alloying effects of Pt-based alloy catalysts for fuel cell applications. *Electrochim. Acta* **2000**, *45* (25), 4211−4217.
(35) Stamenković, V.; Schmidt, T. J.; Ross, P. N.; Marković, N. M. Surface Composition Effects in Electrocatalysis: Kinetics of Oxygen Reduction on Well-Defined Pt_3Ni and Pt_3Co Alloy Surfaces. *J. Phys. Chem. B* **2002**, *106*, 11970−11979.

https://doi.org/10.1021/acs.jpcc.4c06652
J. Phys. Chem. C 2025, 129, 2122−2131

(36) Yano, H.; Kataoka, M.; Yamashita, H.; Uchida, H.; Watanabe, M. Oxygen Reduction Activity of Carbon-Supported Pt−M (M = V, Ni, Cr, Co, and Fe) Alloys Prepared by Nanocapsule Method. *Langmuir* **2007**, *23* (11), 6438−6445.
(37) Zhang, X.; Li, H.; Yang, J.; Lei, Y.; Wang, C.; Wang, J.; Tang, Y.; Mao, Z. Recent advances in Pt-based electrocatalysts for PEMFCs. *RSC Adv.* **2021**, *11* (22), 13316−13328.
(38) Ahn, C.-Y.; Park, J. E.; Kim, S.; Kim, O.-H.; Hwang, W.; Her, M.; Kang, S. Y.; Park, S.; Kwon, O. J.; Park, H. S.; et al. Differences in the Electrochemical Performance of Pt-Based Catalysts Used for Polymer Electrolyte Membrane Fuel Cells in Liquid Half- and Full-Cells. *Chem. Rev.* **2021**, *121* (24), 15075−15140.
(39) Kitchin, J. R.; Nørskov, J. K.; Barteau, M. A.; Chen, J. G. Modification of the surface electronic and chemical properties of Pt(111) by subsurface 3d transition metals. *J. Chem. Phys.* **2004**, *120* (21), 10240−6.
(40) Xu, Y.; Ruban, A. V.; Mavrikakis, M. Adsorption and Dissociation of O_2 on Pt−Co and Pt−Fe Alloys. *J. Am. Chem. Soc.* **2004**, *126* (14), 4717−4725.
(41) Stamenkovic, V. R.; Mun, B. S.; Arenz, M.; Mayrhofer, K. J. J.; Lucas, C. A.; Wang, G.; Ross, P. N.; Markovic, N. M. Trends in electrocatalysis on extended and nanoscale Pt-bimetallic alloy surfaces. *Nat. Mater.* **2007**, *6* (3), 241−247.
(42) Ma, Y.; Balbuena, P. B. Surface Properties and Dissolution Trends of Pt3M Alloys in the Presence of Adsorbates. *J. Phys. Chem. C* **2008**, *112* (37), 14520−14528.
(43) Greeley, J.; Stephens, I. E. L.; Bondarenko, A. S.; Johansson, T. P.; Hansen, H. A.; Jaramillo, T. F.; Rossmeisl, J.; Chorkendorff, I.; Nørskov, J. K. Alloys of platinum and early transition metals as oxygen reduction electrocatalysts. *Nat. Chem.* **2009**, *1* (7), 552−556.
(44) Duan, Z.; Wang, G. A first principles study of oxygen reduction reaction on a Pt(111) surface modified by a subsurface transition metal M (M = Ni, Co, or Fe). *Phys. Chem. Chem. Phys.* **2011**, *13* (45), 20178−20187.
(45) Lim, C.; Fairhurst, A. R.; Ransom, B. J.; Haering, D.; Stamenkovic, V. R. Role of Transition Metals in Pt Alloy Catalysts for the Oxygen Reduction Reaction. *ACS Catal.* **2023**, *13* (22), 14874−14893.
(46) Pillay, D.; Johannes, M. D. Effect of S on Pt(111) and Pt3Ni(111) Surfaces: A First Principles Study. *J. Phys. Chem. C* **2008**, *112* (5), 1544−1551.
(47) Pillay, D.; Johannes, M. D.; Garsany, Y.; Swider-Lyons, K. E. Poisoning of Pt_3Co Electrodes: A Combined Experimental and DFT Study. *J. Phys. Chem. C* **2010**, *114* (17), 7822−7830.
(48) Ke, S.; Qiu, L.; Zhao, W.; Sun, C.; Cui, B.; Xu, G.; Dou, M. Understanding of Correlation between Electronic Properties and Sulfur Tolerance of Pt-Based Catalysts for Hydrogen Oxidation. *ACS Appl. Mater. Interfaces* **2022**, *14* (6), 7768−7778.
(49) Ke, S.; Cui, B.; Sun, C.; Qin, Y.; Zhang, J.; Dou, M. Intriguing H2S Tolerance of the PtRu Alloy for Hydrogen Oxidation Catalysis in PEMFCs: Weakened Pt−S Binding with Slower Adsorption Kinetics. *ACS Appl. Mater. Interfaces* **2022**, *14* (42), 47765−47774.
(50) Watanabe, M.; Motoo, S. Electrocatalysis by ad-atoms: Part III. Enhancement of the oxidation of carbon monoxide on platinum by ruthenium ad-atoms. *Journal of Electroanalytical Chemistry and Interfacial Electrochemistry* **1975**, *60* (3), 275−283.
(51) Wakisaka, M.; Mitsui, S.; Hirose, Y.; Kawashima, K.; Uchida, H.; Watanabe, M. Electronic Structures of Pt−Co and Pt−Ru Alloys for CO-Tolerant Anode Catalysts in Polymer Electrolyte Fuel Cells Studied by EC−XPS. *J. Phys. Chem. B* **2006**, *110* (46), 23489−23496.
(52) Shatkay, A.; Lerman, A. Individual activities of sodium and chloride ions in aqueous solutions of sodium chloride. *Anal. Chem.* **1969**, *41* (3), 514−517.
(53) Rabie, H. R.; Wilczek-Vera, G.; Vera, J. H. Activities of Individual Ions From Infinite Dilution to Saturated Solutions. *J. Solution Chem.* **1999**, *28* (7), 885−913.
(54) Rizo, R.; Herrero, E.; Climent, V.; Feliu, J. M. On the nature of adsorbed species on platinum single-crystal electrodes. *Current Opinion in Electrochemistry* **2023**, *38*, No. 101240.
(55) Garsany, Y.; Baturina, O. A.; Swider-Lyons, K. E. Impact of Sulfur Dioxide on the Oxygen Reduction Reaction at Pt/Vulcan Carbon Electrocatalysts. *J. Electrochem. Soc.* **2007**, *154* (7), B670.
(56) Paál, Z.; Matusek, K.; Muhler, M. Sulfur adsorbed on Pt catalyst: its chemical state and effect on catalytic properties as studied by electron spectroscopy and n-hexane test reactions. *Applied Catalysis A: General* **1997**, *149* (1), 113−132.
(57) Loučka, T. Adsorption and oxidation of sulphur and of sulphur dioxide at the platinum electrode. *Journal of Electroanalytical Chemistry and Interfacial Electrochemistry* **1971**, *31* (2), 319−332.
(58) Clavilier, J.; Armand, D. Electrochemical induction of changes in the distribution of the hydrogen adsorption states on Pt (100) and Pt (111) surfaces in contact with sulphuric acid solution. *Journal of Electroanalytical Chemistry and Interfacial Electrochemistry* **1986**, *199* (1), 187−200.
(59) Itaya, K.; Sugawara, S.; Sashikata, K.; Furuya, N. In situ scanning tunneling microscopy of platinum (111) surface with the observation of monatomic steps. *Journal of Vacuum Science & Technology A* **1990**, *8* (1), 515−519.
(60) Sonsudin, F.; Masuda, T.; Ikeda, K.; Naohara, H.; Uosaki, K. Effect of Coating by Perfluorosulfonated Ionomer Film on Electrochemical Behaviors of Pt(111) Electrode in Acidic Solutions. *Chem. Lett.* **2010**, *39* (3), 286−287.
(61) Wakisaka, M.; Kobayashi, S.; Morishima, S.; Hyuga, Y.; Tryk, D. A.; Watanabe, M.; Iiyama, A.; Uchida, H. Unprecedented dependence of the oxygen reduction activity on Co content at Pt Skin/Pt−Co(111) single crystal electrodes. *Electrochem. Commun.* **2016**, *67*, 47−50.
(62) Suzuki, A.; Nakamura, M.; Hoshi, N. Effects of Surface Structures and Hydrophobic Species on the Oxygen Reduction Reaction Activity of Pt_3Fe Single-Crystal Electrodes. *Electrocatalysis* **2022**, *13*, 175−181.
(63) Ma, Y.; Balbuena, P. B. Pt surface segregation in bimetallic Pt_3M alloys: A density functional theory study. *Surf. Sci.* **2008**, *602* (1), 107−113.
(64) Yu, T. H.; Sha, Y.; Merinov, B. V.; Goddard, W. A., III Improved Non-Pt Alloys for the Oxygen Reduction Reaction at Fuel Cell Cathodes Predicted from Quantum Mechanics. *J. Phys. Chem. C* **2010**, *114* (26), 11527−11533.
(65) Holby, E. F.; Sheng, W.; Shao-Horn, Y.; Morgan, D. Pt nanoparticle stability in PEM fuel cells: influence of particle size distribution and crossover hydrogen. *Energy Environ. Sci.* **2009**, *2* (8), 865−871.
(66) Jinnouchi, R.; Toyoda, E.; Hatanaka, T.; Morimoto, Y. First Principles Calculations on Site-Dependent Dissolution Potentials of Supported and Unsupported Pt Particles. *J. Phys. Chem. C* **2010**, *114* (41), 17557−17568.
(67) Kodama, K.; Nagai, T.; Kuwaki, A.; Jinnouchi, R.; Morimoto, Y. Challenges in applying highly active Pt-based nanostructured catalysts for oxygen reduction reactions to fuel cell vehicles. *Nat. Nanotechnol.* **2021**, *16* (2), 140−147.
(68) Mavrikakis, M.; Hammer, B.; Nørskov, J. K. Effect of Strain on the Reactivity of Metal Surfaces. *Phys. Rev. Lett.* **1998**, *81* (13), 2819−2822.
(69) Kitchin, J. R.; Nørskov, J. K.; Barteau, M. A.; Chen, J. G. Role of Strain and Ligand Effects in the Modification of the Electronic and Chemical Properties of Bimetallic Surfaces. *Phys. Rev. Lett.* **2004**, *93* (15), No. 156801.
(70) Ou, L.; Chen, S. DFT calculation analysis of oxygen reduction activity and stability of bimetallic catalysts with Pt-segregated surface. *Science China Chemistry* **2015**, *58* (4), 586−592.
(71) Oezaslan, M.; Hasché, F.; Strasser, P. $PtCu_3$, PtCu and Pt_3Cu Alloy Nanoparticle Electrocatalysts for Oxygen Reduction Reaction in Alkaline and Acidic Media. *J. Electrochem. Soc.* **2012**, *159* (4), B444.
(72) Jensen, K. D.; Tymoczko, J.; Rossmeisl, J.; Bandarenka, A. S.; Chorkendorff, I.; Escudero-Escribano, M.; Stephens, I. E. L. Elucidation of the Oxygen Reduction Volcano in Alkaline Media using a Copper−Platinum(111) Alloy. *Angew. Chem., Int. Ed.* **2018**, *57* (11), 2800−2805.

https://doi.org/10.1021/acs.jpcc.4c06652
J. Phys. Chem. C 2025, 129, 2122−2131

(73) Zhang, X.; Yu, S.; Zheng, W.; Liu, P. Stability of Pt near surface alloys under electrochemical conditions: a model study. *Phys. Chem. Chem. Phys.* **2014**, *16* (31), 16615−16622.
(74) van den Oetelaar, L. C. A.; Nooij, O. W.; Oerlemans, S.; Denier van der Gon, A. W.; Brongersma, H. H.; Lefferts, L.; Roosenbrand, A. G.; van Veen, J. A. R. Surface Segregation in Supported Pd−Pt Nanoclusters and Alloys. *J. Phys. Chem. B* **1998**, *102* (18), 3445−3455.
(75) Duan, Z.; Wang, G. Monte Carlo simulation of surface segregation phenomena in extended and nanoparticle surfaces of Pt−Pd alloys. *J. Phys.: Condens. Matter* **2011**, *23* (47), No. 475301.
(76) Arenz, M.; Stamenkovic, V.; Schmidt, T. J.; Wandelt, K.; Ross, P. N.; Markovic, N. M. The electro-oxidation of formic acid on Pt−Pd single crystal bimetallic surfaces. *Phys. Chem. Chem. Phys.* **2003**, *5* (19), 4242−4251.
(77) Zheng, Y.; Zhang, L.; He, P.; Dang, D.; Zeng, Q.; Zeng, J.; Liu, M. A Facile and Environmentally Friendly One-Pot Synthesis of Pt Surface-Enriched Pt-Pd(x)/C Catalyst for Oxygen Reduction. *Electrocatalysis* **2018**, *9* (4), 495−504.
(78) Fantauzzi, M.; Atzei, D.; Elsener, B.; Lattanzi, P.; Rossi, A. XPS and XAES analysis of copper, arsenic and sulfur chemical state in enargites. *Surf. Interface Anal.* **2006**, *38*, 922.
(79) Chen, K.; Xue, D. Reaction Route to the Crystallization of Copper Oxides. *Applied Science and Convergence Technology* **2014**, *23*, 14−26.
(80) Seshadri, G.; Xu, H. C.; Kelber, J. A. Sulfur Catalyzed Electrochemical Oxidation of Copper: A Combined Ultrahigh Vacuum Electrochemistry Study. *J. Electrochem. Soc.* **1999**, *146* (5), 1762.
(81) Xu, H. C.; Seshadri, G.; Kelber, J. A. Effect of Sulfur on the Oxidation of Copper in Aqueous Solution. *J. Electrochem. Soc.* **2000**, *147* (2), 558.
(82) Jiang, H.; Yang, H.; Hawkins, R.; Ring, Z. Effect of palladium on sulfur resistance in Pt−Pd bimetallic catalysts. *Catal. Today* **2007**, *125* (3), 282−290.
(83) Stephens, I. E. L.; Bondarenko, A. S.; Perez-Alonso, F. J.; Calle-Vallejo, F.; Bech, L.; Johansson, T. P.; Jepsen, A. K.; Frydendal, R.; Knudsen, B. P.; Rossmeisl, J.; et al. Tuning the Activity of Pt(111) for Oxygen Electroreduction by Subsurface Alloying. *J. Am. Chem. Soc.* **2011**, *133* (14), 5485−5491.
(84) Wu, J.; Shan, S.; Cronk, H.; Chang, F.; Kareem, H.; Zhao, Y.; Luo, J.; Petkov, V.; Zhong, C. J. Understanding Composition-Dependent Synergy of PtPd Alloy Nanoparticles in Electrocatalytic Oxygen Reduction Reaction. *J. Phys. Chem. C* **2017**, *121*, 14128−14136.

https://doi.org/10.1021/acs.jpcc.4c06652
J. Phys. Chem. C 2025, 129, 2122−2131